Available online at www.sciencedirect.com
SCIENCE DIRECT®
Acta Materialia 52 (2004) 2147–2154
Acta MATERIALIA
www.actamat-journals.com

Shock compression response of magnetic nanocomposite powders

Z.Q. Jin [a,b,*], K.H. Chen [a,b], J. Li [a], H. Zeng [b,c], S.-F. Cheng [d], J.P. Liu [b], Z.L. Wang [a], N.N. Thadhani [a]

[a] School of Materials Science and Engineering, Georgia Institute of Technology, Atlanta, GA 30332, USA
[b] Department of Physics, The University of Texas at Arlington, Arlington, TX 76019, USA
[c] IBM T.J. Watson Research Center, Yorktown Heights, NY 10598, USA
[d] Naval Research Laboratory, Washington, DC 20375, USA

Received 11 June 2003; received in revised form 25 December 2003; accepted 5 January 2004

Abstract

The shock compression response of magnetic $Pr_2Fe_{14}B/\alpha$-Fe nanocomposite powders, pressed at different packing densities, was studied in the range of 11–23 GPa shock pressure, using a single-stage gas gun. Bulk compacts (97.5–99% dense) recovered in the form of 12 mm diameter by 4 mm thick disks, were analyzed to determine the structural changes occurring within the particles and at particle boundaries. Scanning electron microscopy observations revealed presence of laminar morphology and strong inter-particle bonding. X-ray diffraction and transmission electron microscopy analysis revealed the retention of nanoscale structure and localized grain refinement. Shear bands were observed and thought to be responsible for the grain refinement. The compact of powders pressed at the intermediate packing density (~76% dense) showed the best densification characteristics, correspondingly, the best magnetic properties with strongest exchange coupling between hard and soft phases.

Keywords: Powder consolidation; Nanocomposite; Hard magnets; Nanostructure; Impact behavior

1. Introduction

Magnetic nanocomposites have attracted much scientific and technological interest in recent years due to their higher remanence and larger theoretical maximum energy product originating from the exchange coupling of magnetic nanosize hard and soft phases. Skomski and Coey [1] first predicted that a giant energy product $(BH)_{max}$ of 1 MJ/m^3 might be attainable in oriented exchange-coupled $Sm_2Fe_{17}N_3/Fe_{65}Co_{35}$ nanocomposites. Similarly, a potential $(BH)_{max}$ of 720 kJ/m^3 was predicted in $Nd_2Fe_{14}B/\alpha$-Fe nanocomposites [2]. These values are about twice that of commercially available anisotropic permanent magnets (~400 kJ/m^3). Of particular importance is that the average grain size of soft magnetic phase in the nanocomposites has to be sufficiently small (5–10 nm) to ensure the exchange interactions between neighboring grains [3]. Many efforts have been made in producing nanocomposite powder particles, thin films, and rapidly quenched flakes through mechanical alloying/milling, sputtering and melt-spinning [4–7]. So far, the attainable $(BH)_{max}$ values (~180 kJ/m^3) [6,7] are still significantly lower than those of above-mentioned predictions. Production of bulk nanocomposites usually results in the decrease of $(BH)_{max}$ due to the practical difficulty of controlling the structure of the material at the nanoscale, while attaining high density in bulk magnets. Conventional consolidation approaches, including resin bonding, extrusion and hot-isostatic-pressing [8], deteriorate the magnetic properties either due to incorporation of non-magnetic binder or by involving prolonged thermal excursions which coarsen the fine nanostructure and destroy the chemical homogeneity.

Consolidation of powders using high-pressure shock waves is a potentially important method for the synthesis and processing of bulk nanocrystalline materials [9–19]. The mechanism of shock consolidation is

* Corresponding author. Tel.: +1-404-894-1475; fax: +1-404-894-9140.
E-mail address: zq.jin@mse.gatech.edu (Z.Q. Jin).

1359-6454/$30.00 © 2004 Acta Materialia Inc. Published by Elsevier Ltd. All rights reserved.
doi:10.1016/j.actamat.2004.01.006

significantly different from that encountered during densification via conventional powder processing techniques. The critical processes occurring during the microsecond time duration of shock compression loading, involve the heterogeneous deposition of shock energy, resulting in interparticle bonding and configurational changes in particles due to the annihilation of voids via plastic flow and dispersion of fragments. Hence, with shock compression, it is possible to fabricate nanocomposite bulk magnets without grain growth since the heating is limited to the particle surface regions and it occurs in the time duration of microseconds. In addition, microstructural modifications and a high density of defects produced under such conditions generate a highly-activated dense-packed state which can result in improvements in properties of bulk shock-consolidated materials [13], or even alter the thermodynamics and kinetics of post-shock crystallization and precipitation treatments to permit retention of metastable phases or nanoscale size of crystallites or precipitates [15].

Recently, powders of single-phase magnetic alloys with nanometer-sized grains have been successfully shock-consolidated (with ~95% of theoretical density) without significant grain growth [18–21]. However, in these studies, the magnetic properties of the compacts prepared under extreme shock loading conditions were found to be lower than those of the pre-compressed powder, possibly either due to excessive thermal effects resulting in local melting or decomposition of the hard phase, or due to stress-induced magnetic phase transition [17,18,20]. Although, it was shown in these studies that shock compression produces bulk magnetic compacts, the control of final compact density and magnetic properties by varying the initial density and shock compression pressure, as well as the mechanism of retaining the nanostructure in the shock-compressed samples, were not fully established. The work conducted in the present study, was thus, focusing on investigating the shock consolidation mechanisms and correlating those to changes in structure and magnetic properties of the recovered compacts as a function of processing characteristics and properties of the nanocomposite starting powders.

2. Experimental procedure

Shock compression experiments were performed using a 3-capsule plate-impact gas-gun fixture [15] on $Pr_2Fe_{14}B$ based nanocomposites powders with α-Fe content of about 20 wt%. The nanocomposites powders in form of ribbon flakes were prepared by melt spinning and subsequent heat treatment at optimal conditions. The ribbon flakes were first comminuted down to 10–200 μm prior to packing in the steel capsules for shock consolidation. The powders were statically pressed in the capsules at different packing densities (~64%, ~76%, and ~78% of theoretical maximum density (TMD)). Impact experiments were conducted using an 80 mm diameter single-stage gas gun equipped with a catch-tank for soft-recovery of shocked samples [14]. To assure well-defined loading conditions, all surfaces incident to the shock direction were mechanically lapped to optical flatness. A 5-mm thick stainless-steel flyer-plate mounted on an aluminum sabot was accelerated using compressed helium gas, at an impact velocity measured to be around 880 m/s. The loading history in these fixtures is dominated by an initial low-pressure planar wave, followed by a radial wave, caused by wave trapping occurring as a result of the low impedance of the powder relative to that of surrounding solid steel containment. To minimize radial wave focusing effects, the shock compression fixtures were designed with a void (air gap) surrounding the capsules. The corresponding maximum peak shock pressures generated upon impact were calculated, using AUTODYN-2D [22] computer code and the P-α model of powder densification [23]. The parameters necessary for AUTODYN-2D simulation were determined by averaging the mass fraction of principal constituents [24]. The corresponding properties for the nanocomposite (80% hard and 20% soft phase) are:

Theoretical maximum density	7.62 g/cm^3
Young's modulus	164 GPa [25,26]
Shear modulus	300 MPa
Yield strength	290 MPa
$U_s - U_p$ shock and particle velocity equation of state	$U_s = 4.056 + 1.446U_p$

Following shock compression, the specimens were recovered in the form of 12 mm diameter by 4 mm thick discs. The densities of these compacts were determined using the Archimedean method, and microhardness measurements were performed using the Leco DM-400F microhardness tester. The starting materials and the recovered shock-consolidated compacts were characterized by X-ray diffraction (XRD) using Cu Kα radiation ($\lambda = 1.54$ Å), scanning electron microscopy (SEM), and transmission electron microscopy (TEM). X-ray diffraction line-broadening analysis, using the Williamson–Hall method [27], was also performed to determine the retained microstrain, and crystallite size reduction. The magnetic properties were measured using a superconducting quantum interference device magnetometer with a maximum applied field of 70 kOe.

3. Results and discussion

3.1. Physical characteristics of shock-consolidated compacts

Table 1 lists the conditions of the recovered compacts following shock consolidation at an impact velocity of

Table 1
The numerical simulation results of shock wave propagation performed using P-α model of densification mechanism

Sample morphology	ρ_{00} (%)	P_I (GPa)	P_O (GPa)	ρ_C (%)	δ (%)	H_V (GPa)
Loose	64	11.5	21.1	97.5	7–13	9–11
Medium	76	14.2	22.7	99	9–14	10–12
Compressed	78	15.1	23.1	98.1	9–14	10–12

Here ρ_{00} is initial density; δ is the compressibility which varies with the shock propagation; P_I and P_O are impact pressures at front surface and output pressure at back surface, respectively; ρ_C is the density of compacts, H_V is the Vickers hardness of consolidated specimens.

880 m/s. The calculated shock pressures, P_I, at the impact surfaces and P_O at the back surfaces of the compacts, represent values obtained from AUTODYNE-2D hydrodynamic code, compiled with P-α model [23] of densification mechanism, as mentioned earlier. It can be seen that the calculated shock pressures are a function of the initial (green) density of the powder, however, in each compact, the pressure at the back surface is almost twice as that at the impact surface. While the radial wave focusing effect was minimized by the provision of a void (air gap) surrounding the powder compact regions, the increase in pressure at the back surface is due to the interaction of the shock wave with the higher-impedance steel backing.

The final compact density ρ_c and compressibility δ measured as change in thickness of ribbons are dependent on the shock pressure and initial packing density. Nearly full densification (∼99%) is obtained in the sample pre-pressed to 76% initial density, while the densification of the 64% and 78% initial density compacts is slightly lower. Table 1 also lists the measured Vicker's microhardness values of the compacts, which scale with the final compact density. The high hardness values (9–12 GPa) of the shock-compacted samples reveal the nature of strong interparticle bonding. No cracking at indentation tips was observed indicating absence of brittle behavior of the shock-consolidated compacts.

3.2. Microstructural characteristics of shock-consolidated compacts

SEM analysis was performed on the fracture surfaces of the compacts to characterize the morphological changes in the powder particles and the nature of interparticle bonding in the shock consolidated samples. Fig. 1 shows SEM micrographs of the starting melt-spun ribbon samples at low and high magnifications and the

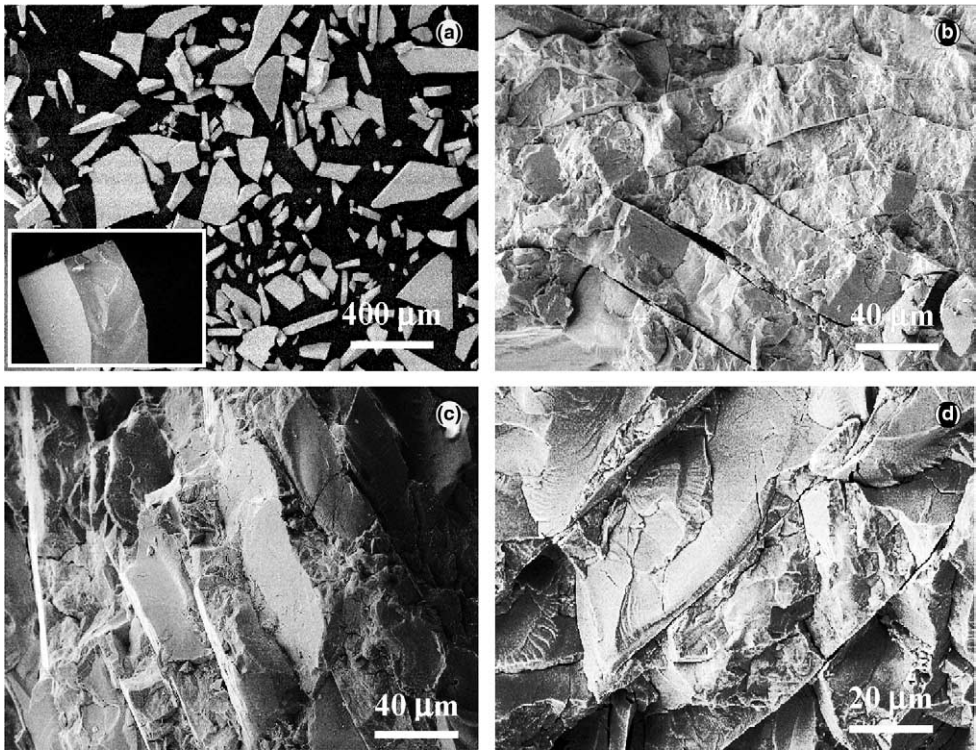

Fig. 1. SEM images of starting materials (a) and shock compressed samples with different initial density. (b) 64 %, (c) 76%, (d) 78%. (Insert in (a) is the high magnification SEM image of single flake.)

fracture surfaces of the compacts in the plane parallel to the shock propagation direction. Shock compression reduces the ribbon thickness down to around 30 μm, indicating a compressibility of 14%, which is in agreement with that obtained from AUTODYN-2D numerical simulations. Because the starting powder is in the form of ribbons, the initial uniaxial pressing causes the flat flakes to become aligned with the flat surfaces perpendicular to the pressing direction. As illustrated in Fig. 1(b)–(d), the flat flakes are seen to retain their alignment even after shock compression. Retention of an aligned nanostructure can be used for development of anisotropic magnets, where an orientation of particles is necessary in the compacts to obtain a high value of the energy product. The enhancement of crystallographic alignment of platelet particles has been reported in superconducting materials where the platelet nature is used to enhance alignment of particles prior to shock compression. [28]

In general, each of the nanocomposite compacts shows extensive plastic deformation and even fracture of some of the ribbons. The compact of the lowest initial packing density reveals the presence of voids between the flakes as shown in Fig. 1(b). The compact of highest initial density shows good interparticle bonding but extensive intraparticle cracking (Fig. 1(d)). However, the intermediate (~76%) initial density compact (and 99% final density) shows the best consolidation with very few voids between particles and minimal intraparticle cracking (Fig. 1(c)). Close observation of the interparticle regions revealed no evidence of melting, which implies that bonding of the ribbon particles was occurring in the solid-state via excessive plastic deformation and flow at the contact surfaces of the particles.

Fig. 2 shows XRD patterns comparing the structure of the starting material and the recovered shock-compacted samples. The diffraction patterns of the starting specimen match the peaks corresponding to those of the 2:14:1 hard-phase and the α-Fe soft-phase. Upon shock compression, the respective peak intensity ratios for both hard and soft phases do not change much, indicating no grain rotation and no preferred texture formation under the shock conditions employed. However, the impact surfaces of all the recovered samples show a broadening of peaks for both magnetic phases, more so for soft α-Fe phase grains. The broadening is related to either microstrain $\Delta d/d$ and/or a decrease in the grain size due to shock compression.

To qualitatively determine the shock-induced configurational changes and effects of shock compression, X-ray diffraction line-broadening analysis was performed on the starting powder and each of the shock-consolidated compacts. The grain (crystallite) size and retained strain were then determined using the Williamson–Hall method [27] as shown in Fig. 3. Each of the compacts shows significant slope indicating considerable retained microstrain in the hard phase, while the starting ribbon powder has no slope and thus no retained strain. The calculated microstrain $\Delta d/d$ in the recovered compacts is determined to be around 4.26–5.36×10^{-3}, which is typical for heavily cold-worked magnetic materials. Values of the crystallite size of the hard phase calculated from the intercept are found to be ~24 nm for the starting ribbon, and 20–22 and 26–29 nm, respectively, for the impact- and rear-surfaces of the recovered shock consolidated specimens. While the grain size measured along the impact surface is slightly smaller than that of the starting ribbon and that of the back surface is slightly larger (possibly due to higher thermal effects), it is important to note the nanoscale (20–30 nm) grain size of the hard phase is indeed retained in each of the compacts throughout their cross-section. The lack of more than two peaks for α-Fe phase made it difficult to calculate its grain size from the Williamson–Hall plot. However, in the case of nanocomposites, the hard $Pr_2Fe_{14}B$ and soft α-Fe phases of

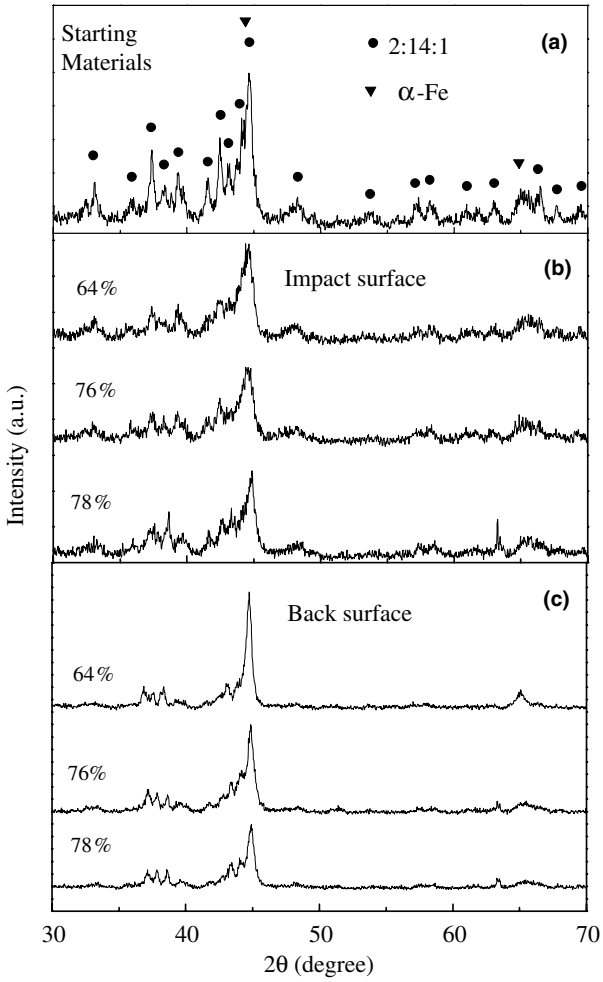

Fig. 2. XRD patterns of (a) starting materials, (b) the impact surface and (c) back surface of shock compressed specimens with different initial density.

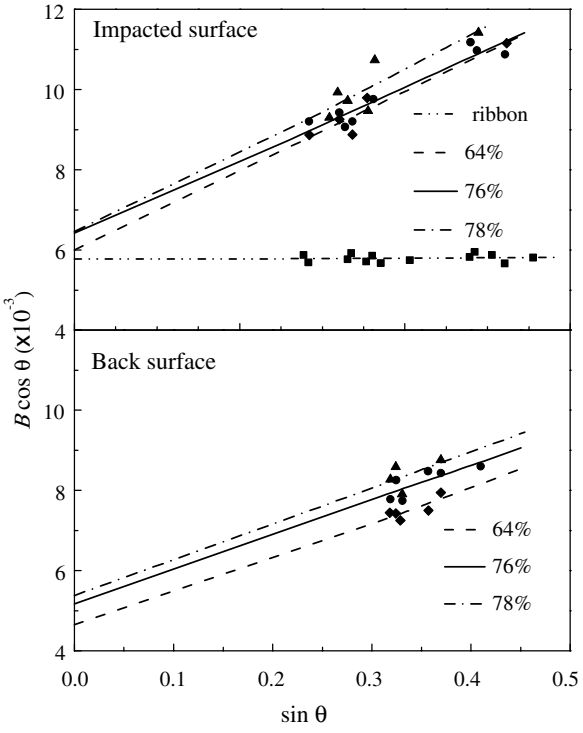

Fig. 3. Williamson–Hall plot comparing impact surface and back surface of the compacts with different initial density. The result of starting materials (ribbons) is shown in upper figure.

nanosized dimensions needed to maintain exchange coupling have local stresses that are not significantly different from each other. Hence, the α-Fe grain size can be estimated by using the value of the hard phase. Correspondingly, the calculated grain size of α-Fe is found to be around 20 nm based on the XRD pattern for the impact surfaces. However, for the back surface, the grain size of α-Fe is slightly larger (30 nm) in the sample with lower initial density than that with higher packing density (25 nm), possibly due to a higher temperature rise associated with the annihilation of a larger volume fraction of voids in the lower-initial-density sample during shock compression.

The effect of shock compression on the retention of nanoscale structure of the retained compacts was also studied in detail using TEM observations. TEM analysis was performed after grinding the compacts into powder form, dispersing them in ethanol, and mounting the particles on a carbon film. Fig. 4(a) and (b) show bright-field TEM images of the starting ribbon material and a shock-densified compact. As shown in Fig. 4(a), the starting ribbon has a mean grain size of ~25 nm; however, some coarse α-Fe grains are also visible. Following shock compression, the grains have a size range of 20–25 nm, as shown in Fig. 4(b), which is consistent with the grain size calculated from XRD line-broadening analysis. The nanoscale grain morphology of the hard magnetic $Pr_2Fe_{14}B$ phase is also conformed by the HRTEM micrograph shown in Fig. 5. The disappearance of large α-Fe grains in the shock-densified compacts appears to be due to fragmentation of the large grains during dynamic compression, which is an important attribute of this technique and has also been reported previously in shock compacted Sm–Fe–N magnets [29].

Shock compression has been shown to introduce large densities of dislocations, point defects, twinning, phase transformation, and shear banding in compacts of microcrystalline powders [9,11,12,16,30]. However, presence of dislocations and twinning was not observed in the shock consolidated nanocomposite powder compacts produced in the present work. A magnetic phase transition, terminated by complete demagnetization of the hard 2:14:1 phase under the longitudinal-shock-wave propagation at 28–38 GPa, was ever discussed [17], although it is not preferred due to its deleterious effect on the magnetic properties of nanocomposite magnets. Such demagnetization effects were also avoided in the present work by using design of recovery fixtures and

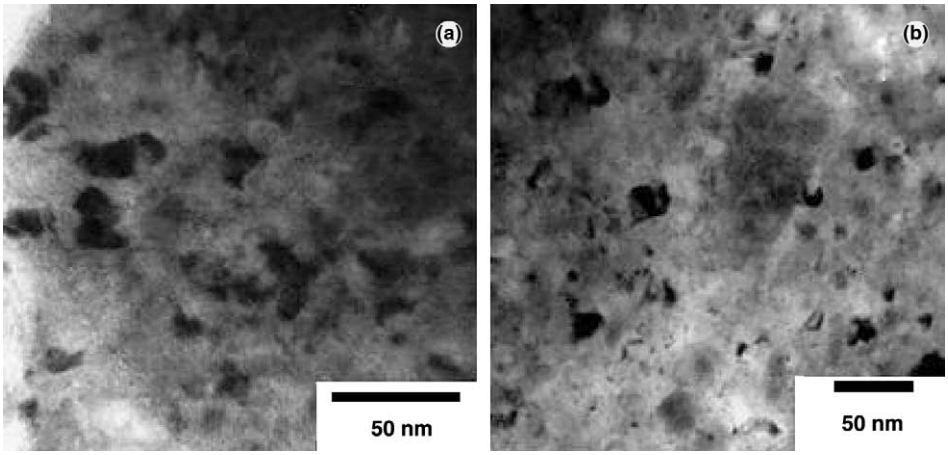

Fig. 4. TEM bright-field micrographs of grain morphology of starting materials (a) and center part of recovered shock-compressed specimens (b).

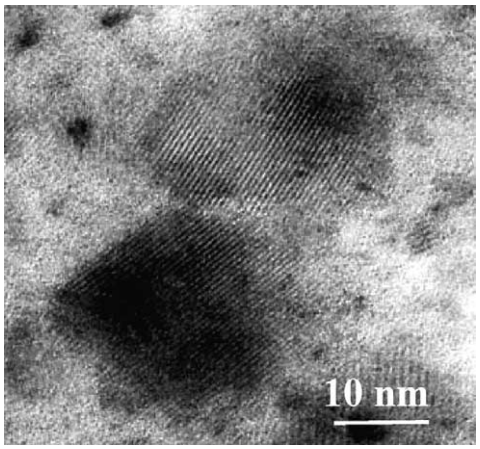

Fig. 5. HRTEM micrographs of $Pr_2Fe_{14}B$ grain morphology of recovered shock-compressed specimens.

use of higher initial packing density to permit control of shock loading conditions. However, an interesting observation in the present work is the existence of shear banding in the recovered shock consolidated compacts. Fig. 6 shows a TEM micrograph illustrating a shear band of several nanometers thickness and hundreds of nanometers in length. The shear band has a shiny appearance quite different from the surrounding matrix due to its different structure where plastic deformation becomes highly concentrated often producing a precursor or path to fracture. It should be noted that it is not easy to observe shear bands if TEM analysis is performed on ground powders of nanocomposite compacts since the compact may be comminuted along shear bands providing the fracture paths. To further investigate the influence of shear bands, additional TEM analysis work is necessary (currently in progress) to more closely identify the structural features in and around the band regions of the nanocomposite compacts.

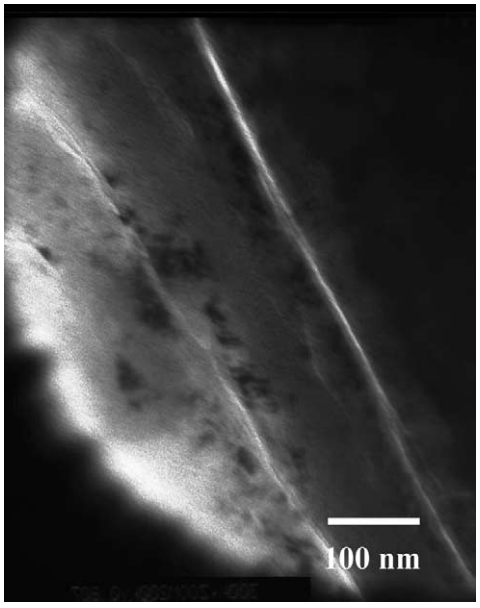

Fig. 6. TEM micrograph illustrating a shear band of several nanometers thickness and hundreds of nanometers in length.

3.3. Magnetic properties of shock-consolidated compacts

The varying shock compression response of nanocomposite powders pressed at different initial packing densities, also leads to a consistent effect on the magnetic properties. Fig. 7 shows the hysteresis loops for the recovered bulk shock consolidated nanocomposite powder compacts of the three different initial packing densities. It can be seen that the change of coercivity H_c is minor and independent of the initial green density. A slight drop in remanence $4\pi M_r$ is observed in the case of the lowest (64%) and highest (78%) initial density compacts compared to that for the intermediate (78%) density compact. Hence, it appears that the magnetic remanence scales with the final compact density, with

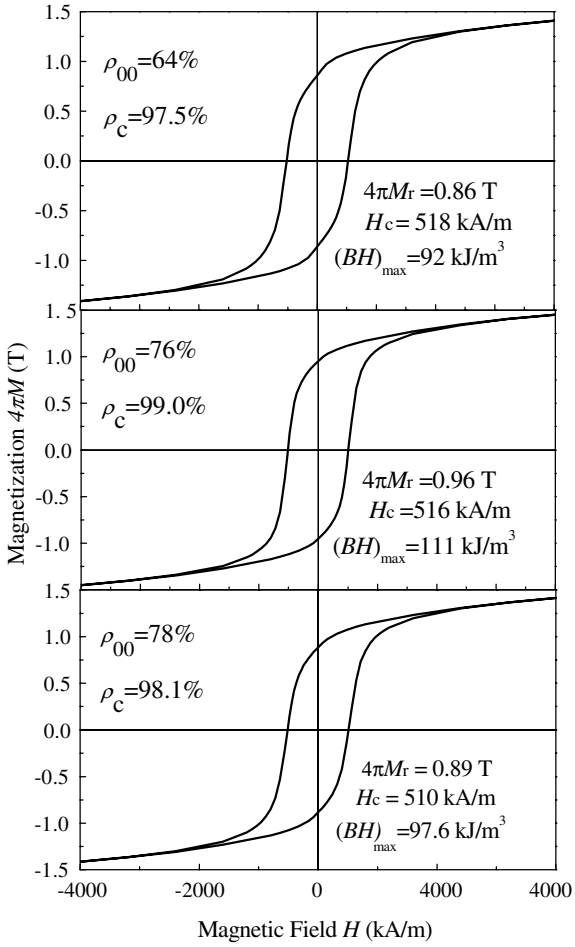

Fig. 7. Hysteresis loops of recovered specimens shocked at 18 GPa and with different initial densities ρ_c and compact densities ρ_c. No demagnetizing calibrations are made with loops.

the 99% dense compact having the highest remanence value ($4\pi M_r = 0.96$ T) and the highest energy product $(BH)_{max} = 111$ kJ/m^3. After considering a demagnetization factor of 1.4, an energy product of 128 kJ/m^3 was obtained, comparable to that of the starting materials. It is noted that the shock compacted nanocomposite magnets possess not only larger density (ρ) but also better magnetic properties than those of commercially available resin-bonded nanocomposite magnets ($\rho \sim$ 80% TMD, $(BH)_{max} \sim 88$ kJ/m^3 for compression molded bonded magnet; and $\rho \sim 68\%$ TMD, $(BH)_{max} \sim 62$ kJ/m^3 for injection molded bonded magnet) since nonmagnetic resins in those bonded magnets results in the decrease of bulk density and therefore the degradation of magnetization and energy products. The optimal magnetic properties achieved in this work are also closely associated with the retention of nanostructure and strong exchange coupling between hard and soft magnetic phases as evidenced by the high remanence ratio ($M_r/M_s > 0.5$). The further grain refinement would provide a potential for significant improvement in magnetic properties. It should also be noted that an increase of coercivity was observed for the samples subjected to subsequent annealing treatment at temperature of 750 °C, which is slightly higher than crystallization temperature. The increase of coercivity may be attributed to the crystallization of pre-existing amorphous phase and formation and retention of nanostructure. The detailed results describing the effect of post-shock heat treatment will be discussed elsewhere.

4. Structure/property correlation with shock compression conditions

In order to understand the effects of initial density on the nanostructural change and magnetic properties, it is necessary to consider the shock loading conditions and shock histories in the nanocomposite powder compact, which are related to the equation of state (EOS) and shock compressibility of the material. The pressure–volume compressibility curves for nanocomposite magnetic powders were calculated based on the Mie-Grüneisen equation of state [23,24], and given as

$$P = \frac{[2V_0 - \gamma_0(V_0 - V)]C^2(V_0 - V)}{[2V_0 - \gamma_0(V_{00} - V)][V_0 - S(V_0 - V)]^2}, \quad (1)$$

where, P is the shock pressure; $1/V_0$ $(= \rho_0)$ and $1/V_{00}$ $(= \rho_{00})$ are the initial density for solid and porous (powder) specimens at ambient pressure; $1/V$ is the density of powder at pressure P; C (~4.056 km/s) is the sound velocity in the nanocomposite; S (~1.446) is the constant characteristic of studied materials, as given in the experimental procedure section. γ_0 is the Grüneisen constant at zero pressure, which can be approximated as $\gamma_0 = 2S - 1$.

By considering the initial density $1/V_0$ of solid nanocomposite to be 7.62 g/cm^3, the P–V curves obtained by applying Eq. (1) on nanocomposites powders can be calculated for the three different initial densities $(1/V_{00})$ and plotted as shown in Fig. 8(a). The P–V curves are very close for the 76% and 78% initial density samples. However, the sample with 64% initial density has a clearly different P–V relation due to the relatively large volume change. Correspondingly, the amount of energy $\{E = 0.5P(V_0 - V)\}$ irreversibly deposited by the shock wave at pressure P is significantly higher for the lowest initial packing density sample as shown in the plot of energy as a function of pressure in Fig. 8(b). The energy deposited by the incident shock converts into an equilibrium shock temperature increase. This explains the higher rise in temperature in the sample with lowest initial packing density, which in turn results in a slightly larger grain size and correspondingly lower magnetic remanence. In case of differences between the impact and back surfaces of the compacts, numerical simulation has shown that the maximum peak shock

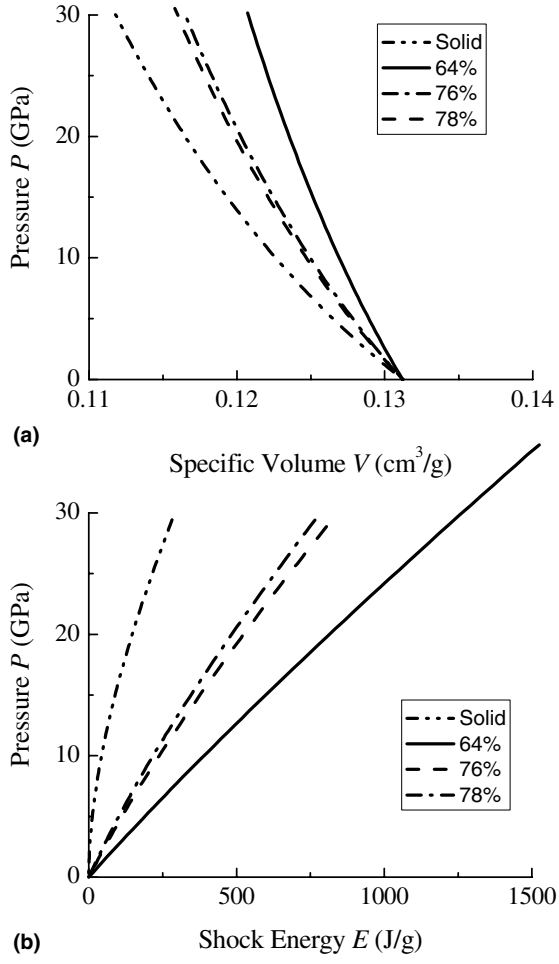

Fig. 8. (a) Schematic of pressure–specific volume curves and (b) calculated shock energy–pressure curves for nanocomposites in solid state and nanocomposites powders with different initial density.

pressure is higher towards the back surface of the compacts, which also implies higher shock energy deposition and correspondingly higher bulk temperature along the back surface of the compact. Therefore, the grains on the back surface of a consolidated compact are slightly larger than those on the impact surface. It should be noted that although high temperatures necessary for adequate metallurgical bonding are produced during shock compression, cooling is attained in time durations too small to cause significant atomic mobility, thereby permitting retention of nanograin size.

Ferromagnetic nanocomposites are two-phase systems in which the small grains of both hard and soft phases behave like single domain particles due to the exchange interaction [7]. It is accepted that in these small grained or ''nano'' composites, the polarization reverses by a mechanism of nucleation and further expansion of inverse domains. These inverse domains nucleate at sites exhibiting a non-uniform magnetization distribution, such as grain boundaries, internal pores and high stress concentrations. Shock compression results in large amounts of microstress that are energetically-preferential locations for the nucleation and growth of inverse domain nuclei, and thus, leads to a slight decrease of coercivity. On the other hand, the refinement of grain size due to shock compression plays an important role in the increase of coercivity and the enhancement of exchange coupling. Therefore, as shown in the present work, the magnetic properties can be retained and even improved in the shock-consolidated samples with appropriate control of shock compression conditions and starting material characteristics.

5. Conclusions

Shock compression processing of nearly full-density bulk nanocomposite magnets starting with different packing characteristics has been performed on mixtures of hard and soft magnetic phases. The investigation of the structural and magnetic properties as function of initial powder packing density shows that proper design of recovery fixtures and controlled packing of powders results in better densification, and retention of nanostructure of both the soft and hard phases. The observed grain refinement is attributed to the formation of shear bands during shock-compression. The compact of powders pressed at the intermediate packing density ($\sim$76% dense) showed the best densification characteristics. Correspondingly, the best magnetic properties with strongest exchange coupling between hard and soft phases were obtained in this powder compact. The wide variance of thermal and mechanical histories experienced during the shock consolidation process and the observed initial density dependence are discussed in terms of the pressure–volume compressibility characteristics with relationships depending on the starting porosity.

Acknowledgements

This work has been supported by US DoD/DARPA through ARO under Grant DAAD-19-01-1-0546. The help of M. McGill, G. Kennedy, L. Ferranti, S. Lieberman, in conducting the gas gun compression experiments at Georgia Institute of Technology is appreciated.

References

[1] Skomski R, Coey JMD. Phys Rev B 1993;48:15812.
[2] Lieneweber T, Kronmüller H. J Magn Magn Mater 1997;176:145.
[3] Fisher R, Schrefl T, Kronmüller H, Fidler J. J Magn Magn Mater 1996;153:35.
[4] McCormick PG, Miao WF, Smith PAI, Ding J, Street R. J Appl Phys 1998;83:6256.
[5] Liu JP, Luo CP, Liu Y, Sellmyer DJ. Appl Phys Lett 1998;72:483.
[6] Jin ZQ, Okumura H, Wang HL, Hadjipanayis GC. J Appl Phys 2002;91:8165.
[7] Goll D, Seeger M, Kronmuller H. J Magn Magn Mater 1998;185:49.
[8] Croat JJ, Herbst JF, Lee RW, Pinkerton FE. J Appl Phys 1994;50:2078.
[9] Thadhani NN. J Appl Phys 1994;76:2129.
[10] Jain M, Christman T. Acta Metall 1994;42:1901.
[11] Verwerft M, Dijken DK, De Hosson JThM, Ven Der Steen AC. Phys Rev B 1994;50:3271.
[12] Meyers MA. Dynamic behavior of materials. New York: Wiley; 1994. p. 382.
[13] Chau R, Maple MB, Nellis WJ. J Appl Phys 1996;79:9236.
[14] Thadhani NN, Graham RA, Royal T, Dunbar E, Anderson MU, Holman TT. J Appl Phys 1997;82:1113.
[15] Counihan PJ, Crawford A, Thadhani NN. Mater Sci Eng A 1999;267:26.
[16] He HL, Sekine T, Kobayashi T. Appl Phys Lett 2002;81:610.
[17] Shkuratov SI, Talantsev EF, Dickens JC, Kristiansen M, Baird J. Appl Phys Lett 2003;82:1248.
[18] Chandramouli M, Thomas G, Nellis WJ. J Appl Phys 1993;73:6494.
[19] Ando S, Mine Y, Takashima K, Itoh S, Tonda H. J Mater Process Tech 1999;85:142.
[20] Mashimo T, Huang X, Hirosawa S, Makita K, Mitsudo S, Motokawa M. J Mater Process Tech 1999;85:138.
[21] Saito T. IEEE Trans Magnet 2001;37:2561.
[22] AUTODYN-2D, Century Dynamics Inc.: Oakland, CA; 1995.
[23] Hermann W. J Appl Phys 1969;40:2490.
[24] Meyers MA. Dynamic behavior of materials. New York: Wiley; 1994. p. 124.
[25] Szymura S, Wyslocki J, Rabinovich Y, Bala H. Phys Stat Sol A 1994;141:435.
[26] Urreta S, Salva H, Ghilarducci A, Billoni O, Fabietti L. Physica B 2002;320:297.
[27] Williamson GK, Hall WH. Acta Metall 1953;1:22.
[28] Seaman CL, Weir ST, Early EA, Maple MB, Nellis WJ, McCandless PC, Brocious WF. Appl Phys Lett 1990;57:93.
[29] Leonowicz M, Kaszuwara W, Jezierska E, Januszewski D, Mendoza G, Davies HA, Paszula J. J Appl Phys 1998;83:6634.
[30] Wongwiwat K, Murr LE. Mater Sci Eng 1978;35:273.